JOURNAL OF MATERIALS SCIENCE **38** (2003) 81–88

A study of the hot formability of an Al-Cu-Mg-Zr alloy

S. SPIGARELLI, M. CABIBBO, E. EVANGELISTA
INFM, Department of Mechanics, University of Ancona, Via Brecce Bianche, 60131, Ancona, Italy
E-mail: spigo@popcsi.unian.it

J. BIDULSKÁ
Department of Metal Forming, Technical University of Košice, Vysokoškolská 4, 040 01, Košice, Slovakia

The high-temperature plasticity of a Zr-stabilised 2014 aluminium alloy was investigated in a wide range of temperatures and strain rates. The microstructure of representative torsioned samples was analysed by transmission electron microscopy, and the characteristics of particle and precipitate distribution were quantitatively estimated. The strain-rate dependence on stress and temperature was analysed by means of the conventional constitutive equations used for describing hot-working behaviour as well as a modified form of the sinh equation, where the stress was substituted by an effective stress, i.e., by the difference between the stress and a threshold stress. This temperature-dependent threshold stress was found to be a fraction of the Orowan stress generated by precipitates increasing from 62 to 94% as temperature decreased from 773 to 573 K.

1. Introduction

The hot formability of Aluminium and its alloys has been extensively evaluated in recent years by means of torsion tests performed in a wide rage of temperatures (473 K to 773 K) and strain rates (10^{-3} to 10 s^{-1}) [1–14]. In the case of pure Aluminium, it was found that the steady-state flow-stress (σ) dependence on testing strain rate ($\dot{\varepsilon}$) can conveniently be described by means of a relationship in the form [15]

$$\dot{\varepsilon} = A(\sinh \alpha\sigma)^n \exp\left(-\frac{Q}{RT}\right) \tag{1}$$

where A and α are material parameters, n is close to 5, and Q is equivalent to the activation energy for self-diffusion in Al. On the other hand, it is well known that when $\alpha\sigma$ is low, i.e., typically in the creep regime, Equation 1 reduces to the conventional power law

$$\dot{\varepsilon} = A^*\sigma^n \exp\left(-\frac{Q}{RT}\right) \tag{2}$$

being A^* a material parameter. Now, it is well established that in the case of pure metals the steady-state creep-rate dependence on the applied stress has the form of a power law with stress exponent close to 5 [16]; this observation suggests that, for pure metals, n should be equal to 5 also when the sinh form is used.

Complex aluminium alloys exhibit a different behaviour; in many cases the activation energy for creep is substantially higher than that for self-diffusion [1–14]. This effect has been attributed to the concurring action of phenomena such as precipitation of strengthening particles, particle-dislocation interaction and, last but not least, coarsening of precipitates. The situation is further complicated by the procedure used for calculating the parameters in Equation 1. The value of α is currently calculated as a best-fit parameter, i.e., by selecting the value that ensures the best linearity, in double log scale, between sinh ($\alpha\sigma$) and $\dot{\varepsilon}$. Since the selection of an α value affects the magnitude of n, the computed stress exponent often assumes very low values ($n = 1$–3) of little physical significance [11].

This study is based on a previous effort to reconcile the different approaches used for describing the low (creep) and high (hot-working) strain-rate regimes [17]; in particular, the attempt is made to elucidate some of the basic features of high-temperature plasticity of a Zr-stabilised 2014.

2. Material and experimental procedures

The 2014 aluminium alloy had the following chemical composition (wt%): Cu = 4.32, Mg = 0.49, Zr = 0.12, Si = 0.68, Fe = 0.23, Mn = 0.77, Ti = 0.03, Al = bal.

Specimens for torsion tests 10 mm in diameter with a gauge length of 20 mm were machined from extruded rods. Torsion tests were carried out at 573, 623, 673, 723 and 773 K on a computer-controlled torsion machine. The equivalent stress σ and the equivalent strain ε were calculated by the relationships:

$$\sigma = \frac{\sqrt{3}M}{2\pi R^3}(3 + m' + n') \tag{3a}$$

$$\varepsilon = \frac{2\pi NR}{\sqrt{3}L} \tag{3b}$$

where R and L are gauge radius and length, respectively, N is the number of revolutions, M is the torque, $m' = (\partial \log M / \partial \log \dot{N})$ at constant strain, and $n' = (\partial \log M / \partial \log N)$ at constant strain rate. For the peak-stress condition, clearly $n' = 0$ and, for the sake of simplicity, m was also taken equal to 0. The simplified formula used for σ does not take into account the gradients in strain and strain rate, which tend to increase σ by less than 10%.

The surface equivalent strain rates were 10^{-3}, 2×10^{-3}, 10^{-2}, 2×10^{-2}, 10^{-1}, 2×10^{-1} and 1 s^{-1}. The samples were heated to the testing temperature in air by a frequency-induction coil. The temperature was measured by an internal thermocouple in close proximity to the gauge, since preliminary measurements confirmed that this configuration of the control thermocouple does not result in any significant temperature gradient along the gauge length. Prior to testing, heating at 1 K/s from room to the desired temperature was followed by 300 s of temperature stabilisation. After rupture samples were quenched with water jets to avoid microstructure modifications during slow cooling from the testing temperature.

Specimens for transmission electron microscopy (TEM) were ground to a thickness of about 100 μm, then discs were prepared by means of double-jetting with a solution of 1/3 HNO_3 in methanol at $-35°C$, 20 V and a current of 40–50 mA/mm^2.

3. Experimental results

3.1. Flow stress in torsion

Plots of equivalent stress vs. equivalent strain under various testing conditions are illustrated in Fig. 1. The curves exhibit a peak, followed by a moderate flow softening up to a steady state. At the highest temperatures under the lowest strain rate, the curves have an almost parabolic shape, the peak being reached at strains close to 1 after a prolonged strain-hardening stage. Fracture strains are shown in Fig. 2; in general, ductility increases with temperature; between 623 and 773 K rupture strain increases with strain rate up to a maximum for $\dot{\varepsilon} \approx 10^{-1}$–1 s^{-1}.

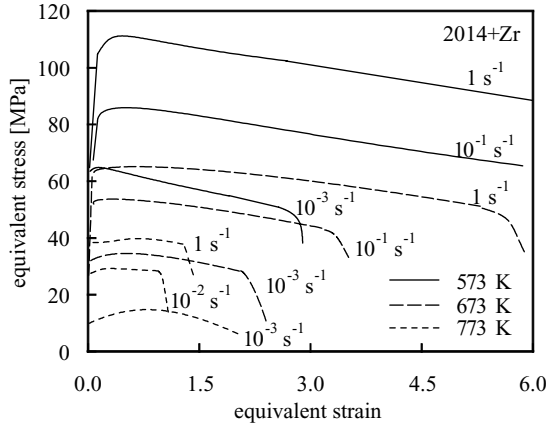

Figure 1 Equivalent-stress vs. equivalent-strain curves.

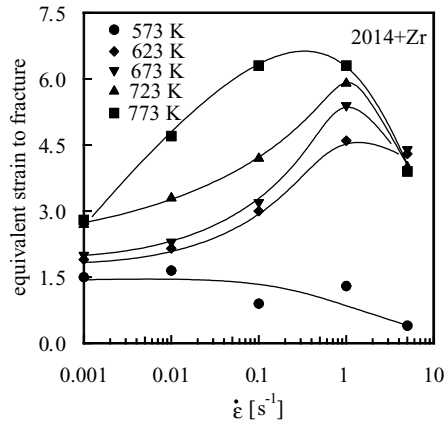

Figure 2 Ductility as a function of testing condition.

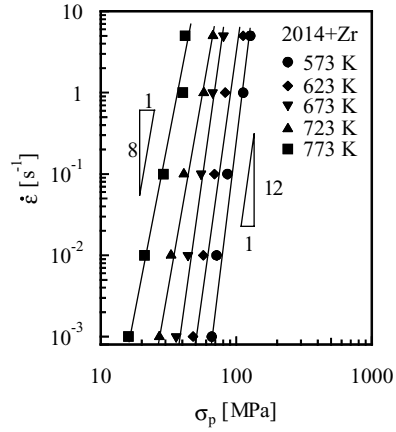

Figure 3 Strain-rate vs. peak-flow stress.

Fig. 3 illustrates the peak flow stress as a function of strain rate; the strain-rate sensitivity of flow stress m ($m = (\partial \log \sigma / \partial \log \dot{\varepsilon})$) increases with temperature.

3.2. Microstructure

Fig. 4 shows the typical microstructure of torsioned samples at low magnifications; the microstructure consists of chains of equiaxed or slightly elongated subgrains that developed inside the elongated grains.

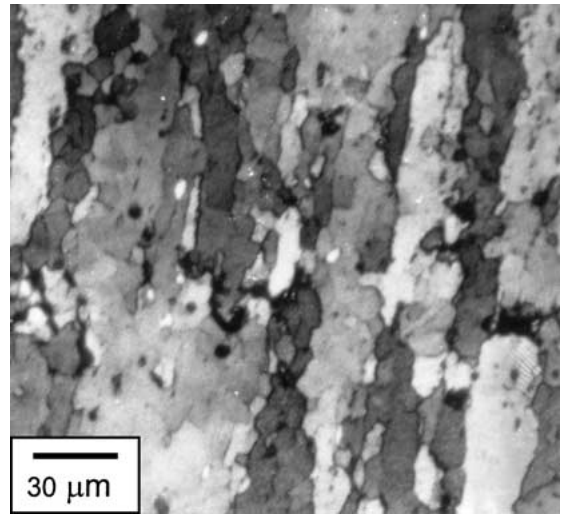

Figure 4 Microstructure of a torsioned sample (773 K-5 s^{-1}) (light microscopy).

TABLE I Equivalent diameter (d), number per volume unit (N_V) of particles and Orowan stress for torsioned samples. The average value of Orowan stress at each temperature was used to estimate the K parameter in Equation 10

Temperature (K)	Strain rate (s^{-1})	d (nm)	N_v (10^{18} m^{-3})	σ_{Or} (MPa)
573	10^{-3}	71	14.6	34.0
573	10^{-2}	75	14.8	36.3
573	10^{-1}	58	14.8	28.9
673	10^{-3}	67	15.3	30.7
673	10^{-2}	72	12.2	29.0
673	10^{-1}	77	17.0	36.9
773	10^{-3}	78	14.6	31.6
773	10^{-2}	76	15.7	32.0
773	10^{-1}	65	22.3	34.0

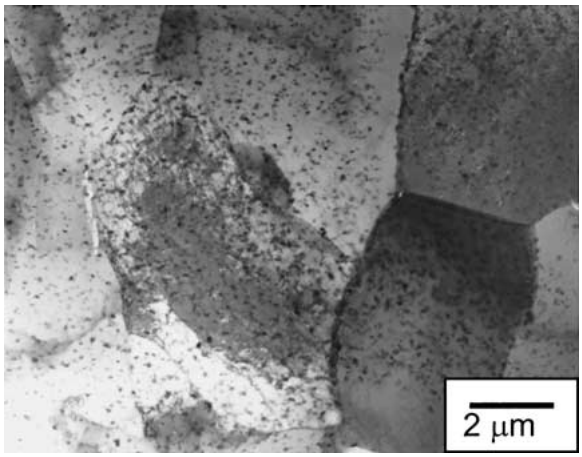

Figure 5 Microstructure of the sample deformed at 773 K-10^{-2} s^{-1}; the substructure formed inside elongated grains is well documented.

TEM inspection of the microstructure of the samples tested at different temperatures under different strain rates (Figs. 5 and 6) revealed the presence of a dispersion of precipitates within the grains. Even at the highest temperature, closely corresponding to the solution-treatment temperature [18], the subgrain interior showed a distribution of fine precipitates. Considerable dislocation interaction with all the fine precipitates was also observed, revealing their hardening effect. The average equivalent diameter (d) and the number per volume unit (N_V) of the hardening particles were calculated for each condition (Table I). The histograms presented in Fig. 7 illustrate the size distribution of precipitates at 673 and 773 K; it can easily be observed that at 773 K, for the lowest strain rate, the frequency of the fine precipitates is lower than in the other conditions; this effect can be attributed to the dissolution of the finest particles.

The micro-hardness and the electrical conductivity of torsioned samples is plotted in Fig. 8. The analysis of Fig. 8a shows that hardness increases with temperature, an effect of solid-solution hardening; this conclusion is supported by the progressive reduction in conductivity with increasing temperature and decreasing strain rate noted in Fig. 8b. The hardness increase observed with increasing strain rate should rather be attributed to dislocation hardening; in fact, as strain rate increases, the structure becomes progressively less recovered, as

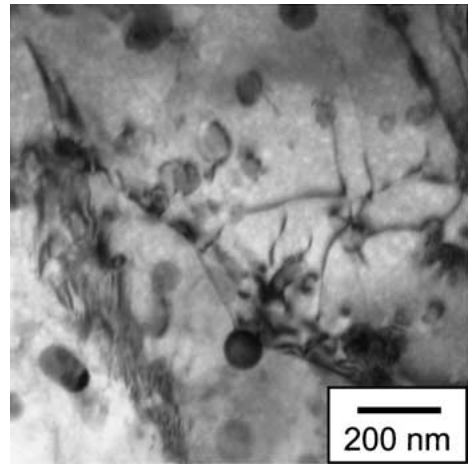

(a)

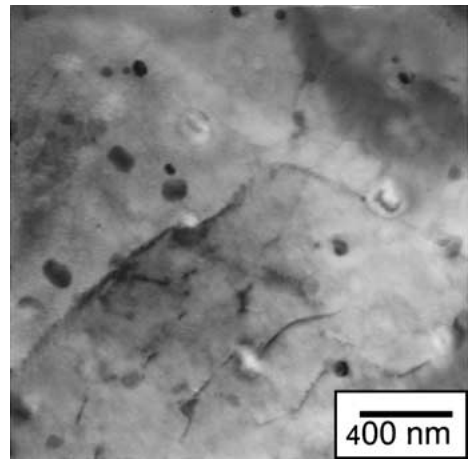

(b)

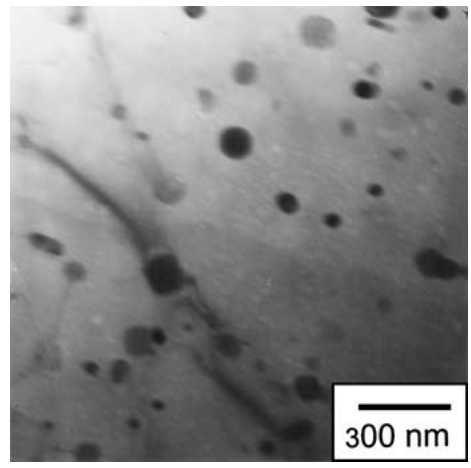

(c)

Figure 6 Microstructure of samples tested at: 573 K-10^{-3} s^{-1} (a); 773 K–10^{-3} s^{-1} (b) and 773 K- 10^{-1} s^{-1} (c).

confirmed by the finer subgrain size usually observed in this range of testing conditions [11]. A comparison between the hardness measured along the gauge length of deformed samples (as a function of time in temperature, i.e., of stabilisation and testing time) and that measured after a T6 treatment is plotted in Fig. 9. Strained samples are usually softer than overaged or even solution-treated ones, the hardness of sample deformed at low strain rate at 773 K being similar to that measured after a simple solution treatment. The very modest hardness of the 2014 + Zr alloy as received clearly indicates that

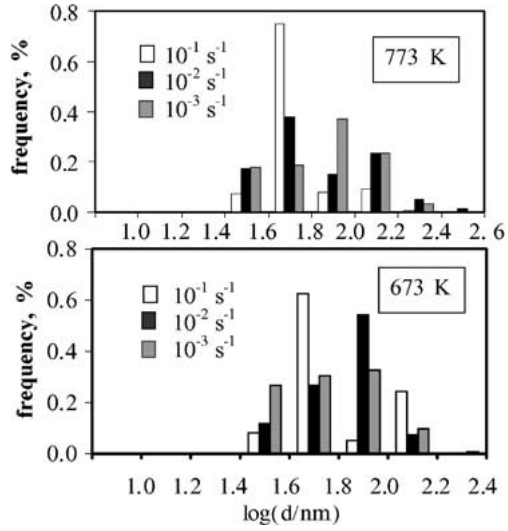

Figure 7 Relative frequency of particle-size distribution at two different testing temperatures.

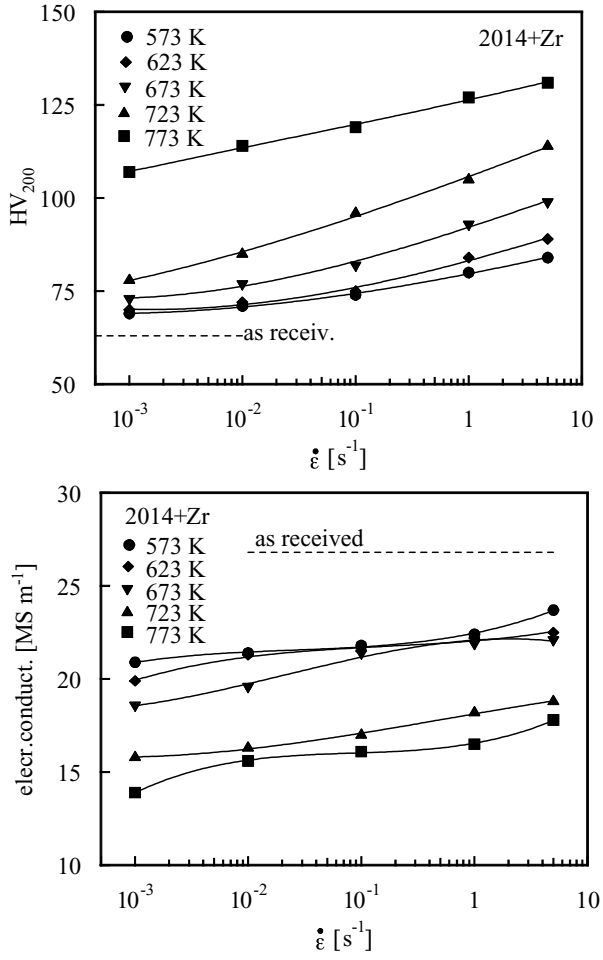

Figure 8 Hardness measured along the gauge length near the surface (a), and electrical conductivity (b) of torsioned samples as a function of strain rate.

the initial state is similar to a stabilised microstructure. It must necessarily be concluded that the initial, soft structure is progressively hardened by the dissolution of few precipitates, even though the very short time of exposure cannot be expected to fully dissolve the precipitated phases. Rather, the analysis of Table I shows a moderate variation of the volume fraction of intragranular precipitates.

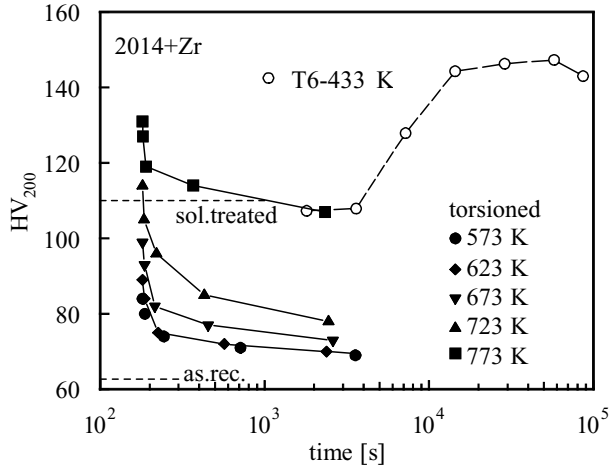

Figure 9 Comparison between the hardness measured on torsioned sample, and that measured on the same alloy in the as received condition, after solution treatment and after ageing; the time, in the case of torsioned samples, represent the sum of testing and temperature-stabilisation durations.

3.3. Constitutive relationships

The relationship between maximum stress, strain rate and temperature was preliminarily described by the well-known equation

$$Z = \dot{\varepsilon} \exp\left(\frac{Q}{RT}\right) = A(\sinh \alpha\sigma)^n \qquad (4)$$

being Z the Zener-Hollomon parameter; Q is obtained from the slope S in an Arrhenius-type plot by the equation

$$Q = 2.3nRS \qquad (5)$$

The use of the sinh function instead of the conventional power law serves to make the constant T data linear, as power-law breakdown results in a decrease in m at high strain rates. However, changing the value of α causes n and Q to vary accordingly; in particular an increase in α invariably corresponds to a decrease in n. Fig. 10 shows an example of the plots used to calculate the

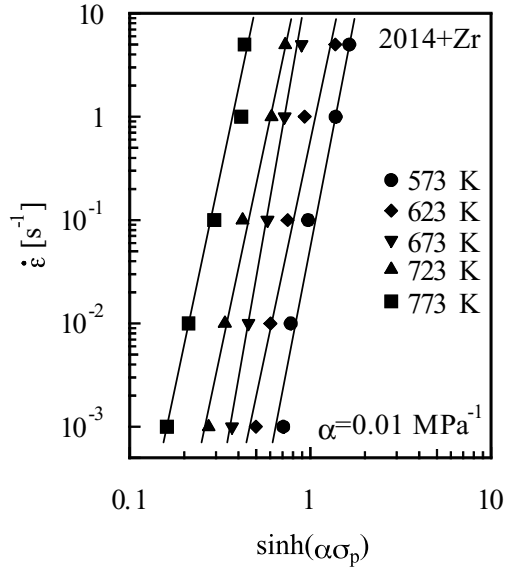

Figure 10 Plot used for the calculation of $\bar{n}$ ($\alpha = 0.01$ MPa^{-1}).

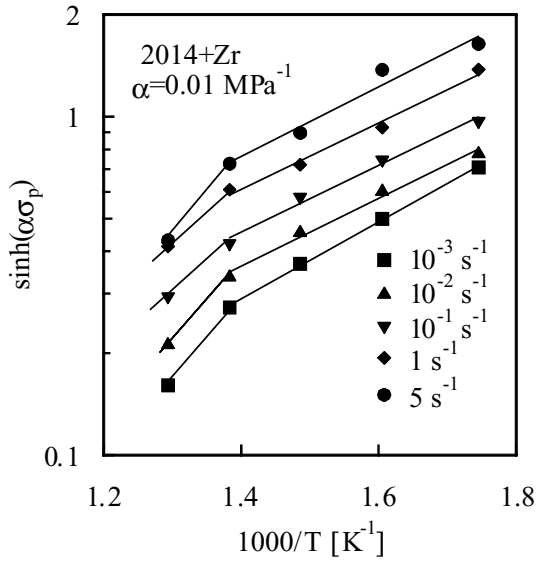

Figure 11 Plot used for calculating the activation energy ($\alpha = 0.01$ MPa^{-1}).

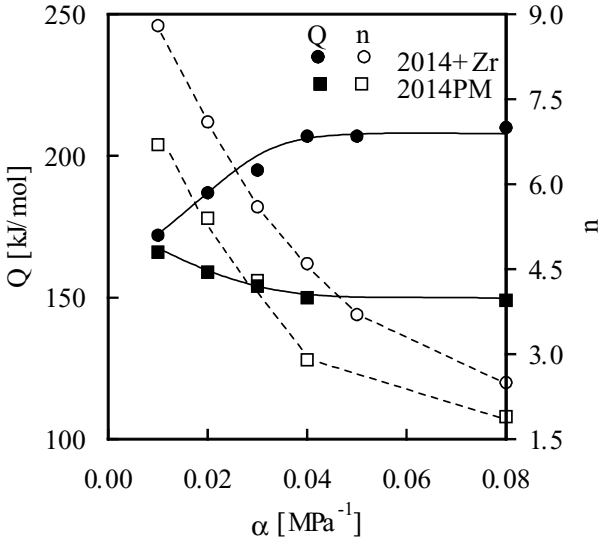

Figure 12 Effect of the selection of α values on the magnitude of the calculated Q and $\bar{n}$ values.

average values of n ($\bar{n}$) and S ($\bar{S}$), in this case, being $\alpha = 0.01$ MPa^{-1}. The same analysis was repeated using α values ranging from to 0.01 to 0.08 MPa^{-1}; the plot used for calculating the activation energy is shown in Fig. 11. Apparently, two different regimes exist: a low-temperature regime ($T \leq 723$ K), where the activation energy is relatively constant for a given α value, and a high-temperature regime ($T = 773$ K) characterised by a higher value of the activation energy.

The changes in $\bar{n}$ and Q (low-temperature regime) as a function of α are illustrated in Fig. 12. It can clearly be observed that an increase in α corresponds to a continuous decrease in $\bar{n}$, while the activation energy Q decreases at first, then remains constant for $\alpha > 0.04$ MPa^{-1}. For comparison purposes, the corresponding trends obtained by testing a 2014 alloy produced by powder metallurgy [17] after 24 h stabilisation at the torsion temperature are reported in the same figure. The plot in Fig. 12 suggests that the selection of different α values, provided that $\alpha > 0.04$ MPa^{-1},

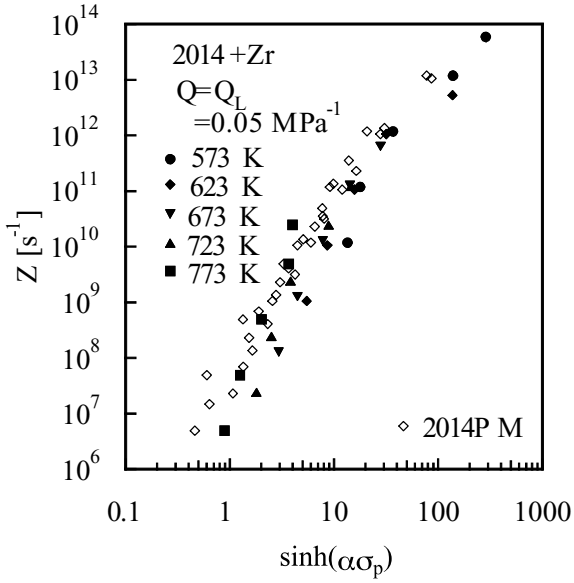

Figure 13 Zener-Hollomon plot (with Q = activation energy for self-diffusion) for the 2014 + Zr alloy and the 2014PM alloy tested in [14].

does not affect the calculation of the activation energy. In this sense, the selection of $\alpha = 0.05$ MPa^{-1} appears to be fully justified, since it compares very well with the "traditional" value of $\alpha = 0.052$ MPa^{-1} [11]. Fig. 13 plots the Zener-Hollomon parameter with $Q = Q_L = 143.4$ kJ/mol (activation energy for self-diffusion in Al) [19] as a function of the sinh ($\alpha\sigma$) with $\alpha = 0.05$ MPa^{-1} for the 2014PM [17] and the alloy of the present study. It is easy to see that the data, particularly at high and low strain rates, do not lie on a single line, as would be expected, but rather over a quite large scatter band.

4. Discussion

4.1. Constitutive equations

The empirical nature of Equation 1 when used to describe the hot-working behaviour of complex alloys is fully evidenced by the unsatisfactory description reported in Fig. 12. In fact, for pure metal or class-M alloys, below power-law breakdown the strain-rate dependence on stress can simply be described by means of a conventional power law with stress exponent $n = 5$; yet, when $\alpha\sigma < 0.8$, Equation 1 reduces to a power law with exponent n, and the activation energy is equivalent to the activation energy for self-diffusion. For pure metals and class-M materials, the value of the n constant in Equation 1 should thus coincide with the theoretical value of $n = 5$; as mentioned above, this is not the case of the alloy of the present study, and of many other Al alloys [1–14] even when the calculated Q values are reasonably close to the activation energy for self-diffusion in Al. In the high strain-rate regime, the use of Equation 1, with the values of n resulting from the selection of the optimum α value giving the best linearity in a $\log(\dot{\varepsilon})$ vs. $\log(\sinh \alpha\sigma)$ plot, can give satisfactory results; nevertheless, lower strain-rate data cannot reasonably be expected to lie invariably on the same straight line of slope $n = 1.5$–2.5. The inadequacy of Equation 1 in giving an accurate and physically sound description of low strain-rate data when the computed

n value is 1.5–2.5 has been demonstrated in the analysis of creep and torsion data obtained by testing the 2014 alloy produced by powder metallurgy [17]. In fact, for PM materials m tends to decrease with decreasing strain rate, a behaviour that cannot be described by Equation 1. By analogy with particle-strengthened alloys, where the applied stress in the power law is conveniently substituted by the an effective stress, that is the difference between the applied stress and a threshold stress σ_0, Equation 1 can be rewritten in the form

$$\dot{\varepsilon} = A_0\left[\sinh\alpha'\left(\frac{\sigma-\sigma_0}{G}\right)\right]^n \exp\left(-\frac{Q}{RT}\right) \quad (6)$$

Equation 6 reduces to

$$\dot{\varepsilon}\propto\left(\frac{\sigma-\sigma_0}{G}\right)^n \exp\left(-\frac{Q}{RT}\right) \quad (7)$$

when $\alpha'(\sigma-\sigma_0)/G < 0.8$; n, in both Equations 6 and 7, should be = 3 or 4–5. Analysis of the creep data for the 2014PM alloy has allowed to estimate the threshold stress with sufficient accuracy, leading to conclude that deformation ($n = 3$) at 773 and 723 K was controlled by viscous glide whereas at the lowest temperature ($n = 5$) climb was the rate-controlling mechanism; in this regime, the best description of the experimental data was obtained for $\alpha' = 305$ [17].

In the case of the alloy of the present study, the direct calculation of the threshold stress is precluded by the lack of very low strain-rate (creep) data. Nevertheless, an attempt was made by simply substituting $\alpha' = 305$ and $n = 5$ at $T = 573$–673 into Equation 6, and using $n = 3$ at $T = 723$–773 K. The resulting equations were then used to fit the experimental data (Fig. 14), obtaining an estimation of the threshold stresses; the fitting of the data, as shown in Fig. 14a, is excellent. Fig. 14b shows the plot of the term $A_T = A_0\exp(-Q/RT)$, obtained by best fitting, as a function of the reciprocal absolute temperature ($T = 573$–673 K). The computed Q value is reasonably close to the activation energy for self-diffusion.

Obviously, the assumption of a constant value of threshold stress at a given temperature is an oversimplification; as mentioned above, at the higher temperatures the progressive dissolution of precipitates should lead to a marked decrease in threshold stress, particularly when the strain rate is low. Yet, for strain rates exceeding 10^{-3} s^{-1}, the testing time corresponding to the peak stress is at least of one order of magnitude lower that the duration of temperature stabilisation; thus, it can reasonably be assumed that in the majority of tests the volume fraction and size of the precipitates is fairly similar, since it is the result of the dissolution of particles that took place during the 300 s at the testing temperature before torsion. This assumption is in agreement with the data reported in Table I.

The temperature-compensated strain rate Z as a function of the non-dimensional effective stress is plotted in Fig. 15 for both the present alloy and the 2014PM alloy. The selection of $Q = 143.4$ kJ mol^{-1} to calculate the temperature-normalised strain rate is justified by its similarity to the activation energies for diffusion

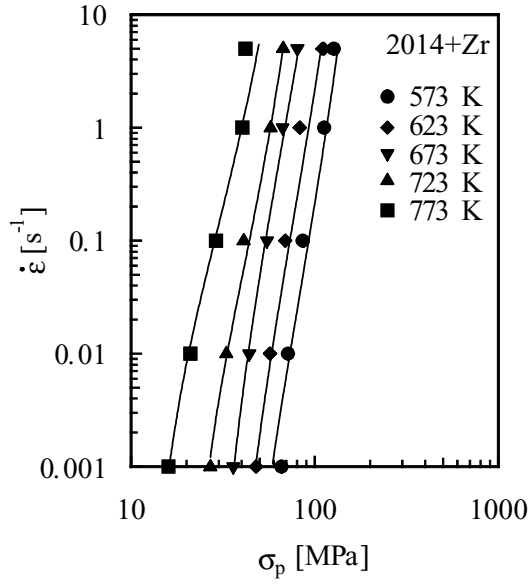

(a)

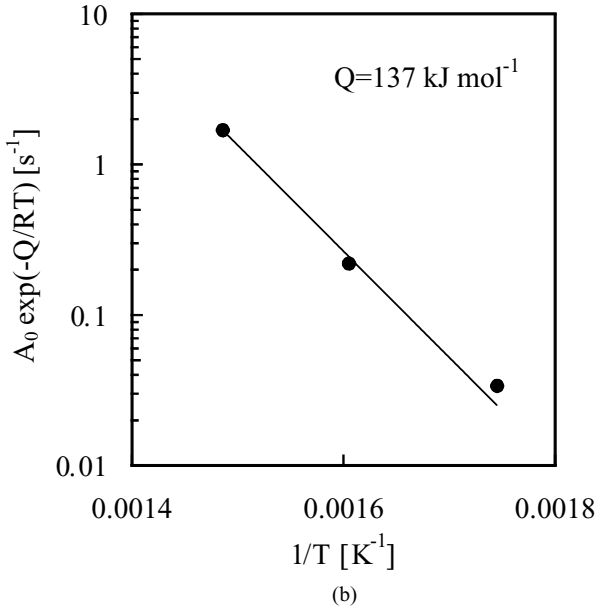

(b)

Figure 14 Strain rate vs. peak flow stress described by means of Equation 6 (a); the Arrhenius-type plot in (b) was used to calculate the true activation energy.

of Mg (130 kJ/mol) and Cu (126 kJ/mol) in Al [20]. As expected, Fig. 15 clearly shows that climb is rate-controlling in the low-temperature regime (573–623 K) and in the high strain-rate region at 673 and 723 K. At these temperatures in the low strain-rate regime, and practically in the whole range of strain rates investigated at 773 K, viscous glide is the rate-controlling mechanism (i.e., $n = 3$) [19]. Quite interestingly, the two sets of data almost overlap, indicating that, even though the nature of the precipitates and their size and distribution are different (in PM alloys there is an additional dispersion of fine oxide particles), the same mechanisms operate in these alloys of similar composition.

Fig. 16 plots the calculated values of the threshold stresses as a function of temperature. The modulus-compensated threshold stress exhibits a weak dependence on temperature; only at 773 K, does the partial dissolution of dispersed phases result in its marked decrease.

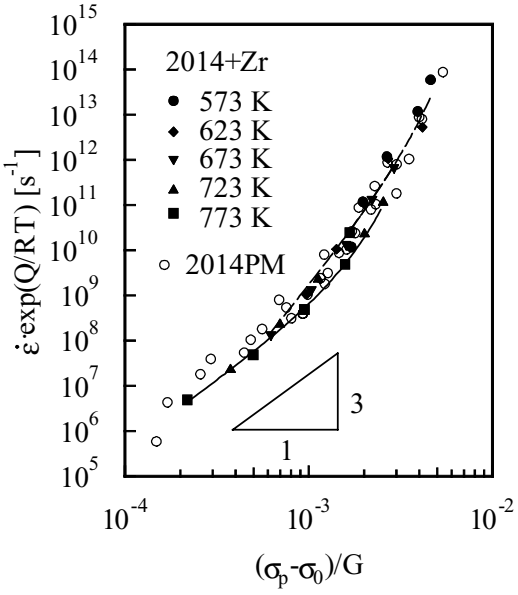

Figure 15 Zener-Hollomon parameter as a function of the non-dimensional effective stress for the 2014 + Zr alloy and the 2014 PM alloy tested in [17].

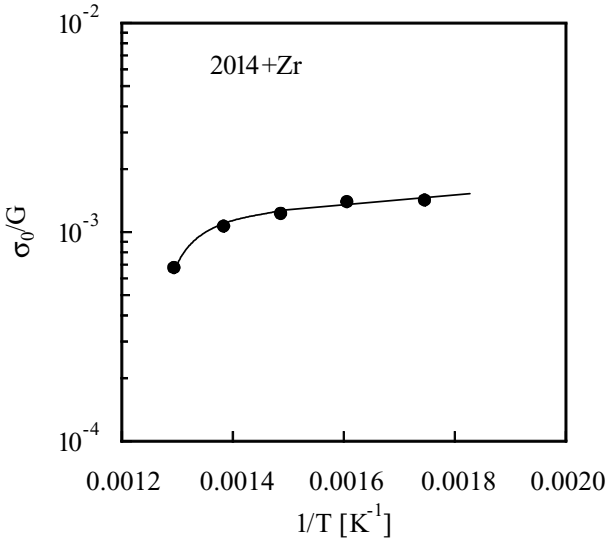

Figure 16 Variation of the threshold stress with temperature.

4.2. Microstructure and threshold stress

The nature of the threshold stress in complex alloys produced by powder metallurgy or ingot casting has been investigated in several studies [21–30]. In alloys produced by casting, it has been attributed to the interaction between dislocation and fine incoherent precipitates [29–30]. In the case of the present study, the dispersion of fine precipitates represents an effective obstacle to dislocation motion; as a result, there should exist a direct correlation between particle size spacing and threshold stress. Table I reports the magnitude of threshold stress, calculated by the relationship [31]:

$$\sigma_{\mathrm{Or}} = \frac{0.81MGb}{2\pi(1-\nu)^{1/2}} \frac{\ln(d/b)}{(\lambda - \sqrt{2/3}d)} \tag{8}$$

where ν is Poisson's ratio and M is the Taylor factor, and

$$\lambda = \frac{1}{2\sqrt{N_v d}} \tag{9}$$

The comparison between threshold and Orowan stress reveals that

$$\sigma_0 = K\sigma_{\mathrm{Or}} \tag{10}$$

where $K = 0.92 \pm 0.11$, 0.75 ± 0.09 and 0.37 ± 0.01 at 573, 673 and 773 K, respectively. This result can favourably be compared with the one obtained by testing the 2024PM alloy in creep where, with the Orowan stress expressed by Equation 8, $K \approx 0.94$, 0.84 and 0.62 at 548, 573 and 603 K [24], although in this case the Orowan stress was calculated by taking into account only fine particles ($d < 150$ nm).

5. Conclusions

The high-temperature plasticity of a 2014 + Zr aluminium alloy was investigated in a wide range of temperatures and strain rates by means of torsion tests. The strain-rate dependence on stress and temperature was described by means of a modified form of the sinh equation, where the peak flow stress (or the applied stress, in the case of creep tests) was substituted by the effective stress, i.e., the difference between peak stress and a threshold stress. This temperature-dependent threshold stress was found to be a fraction (62–94%) of the Orowan stress generated by the dispersion of precipitated phases.

Acknowledgements

The authors greatly acknowledge Mr. D. Ciccarelli (Univeristy of Ancona, Department of Mechanics) for his precious co-operation in experimental activity.

References

1. H. J. McQUEEN and J. J. JONAS, in "Metal Forming: Interrelation Between Theory and Practice," edited by A. L. Hoffmanner (Plenum, New York, 1971) p. 393.
2. H. J. McQUEEN, E. EVANGELISTA, N. JIN and M. E. KASSNER, *Metall. Mater. Trans.* A **26A** (1995) 1757.
3. H. J. McQUEEN, E. EVANGELISTA and M. E. KASSNER, *Z. Metallkde.* **82** (1995) 336.
4. E. EVANGELISTA, F. GABRIELLI, P. MENGUCCI and E. QUADRINI, in "Strength of Metals and Alloys," edited by P. O. Kettunen, T. K. Lepisto and M. E. Lehtonen (Pergamon Press, Oxford, UK, 1988) p. 977.
5. E. EVANGELISTA, E. DIRUSSO, H. J. McQUEEN and P. MENGUCCI, in "Homogenization and Annealing of Aluminium and Copper Alloys," edited by H. D. Merchant, J. Crane and E. H. Chia (The Minerals, Metals and Material Society, Warrendale, PA, 1988) p. 209.
6. H. J. McQUEEN, in "Hot Deformation of Aluminum Alloys," edited by T. G. Langdon, H. D. Merchant, J. G. Morris and M. A. Zaidi (The Minerals, Metals and Material Society, Warrendale, PA, 1991) p. 31.
7. *Idem.*, in "Hot Deformation of Aluminium Alloys," edited by T. G. Langdon, H. D. Merchant, J. G. Morris and M. A. Zaidi (The Minerals, Metals and Material Society, Warrendale, PA, 1991) p. 105.
8. H. J. McQUEEN and J. J. JONAS, in "Microstructural Control in Aluminium Alloys," edited by C. Q. Quen *et al.* (TMS-AIME, Warrendale, PA, 1986) p. 197.
9. E. EVANGELISTA, H. J. McQUEEN and E. CERRI, in "Modelling of Plastic Deformation and its Engineering Applications," edited by S. I. Andersen *et al.* (Risø National Laboratory, Roskilde, DK, 1992) p. 265.
10. L. BLAZ and E. EVANGELISTA, *Mater. Sci. Eng.* A **207** (1996) 195.

11. E. CERRI, E. EVANGELISTA, A. FORCELLESE and H. J. MCQUEEN, *ibid.* **197** (1995) 181.
12. H. J. MCQUEEN and J. J. JONAS, in "Plastic Deformation of Materials," Vol.6, edited by R. J. Arsenault (Academic Press, New York, 1975) p. 393.
13. E. EVANGELISTA, A. FORCELLESE, F. GABRIELLI and P. MENGUCCI, in "Hot Deformation of Aluminium Alloys," edited by T. G. Langdon, H. D. Merchant, J. G. Morris and M. A. Zaidi (The Minerals, Metals and Material Society, Warrendale, PA, 1991) p. 121.
14. E. CERRI, E. EVANGELISTA, A. FORCELLESE, P. FIORINI and J. STOBRAWA, in "Strength of Metals and Alloys," edited by H. Oikawa *et al*. (The Japan Institute of Metals, Tokyo, 1994) p. 807.
15. H. J. MCQUEEN and J. J. JONAS, *Manufacturing Eng. Trans.* **2** (1973) 209.
16. M. E. KASSNER and M.-T. PEREZ-PRADO, *Prog. Mat. Sci.* **45** (2000) 6.
17. E. EVANGELISTA and S. SPIGARELLI, *Metall. Trans.* **33A** (2002) 373.
18. P. OLAFFSON and R. SANDSTROM, *Mat. Sci. Tech.* **17** (2001) 655.
19. F. A. MOHAMED and T. G. LANGDON, *Metall. Trans.* **5** (1974) 2339.
20. S. MROWEC, in "Defects and Diffusion in Solids" (Elsevier, Amsterdam, 1980) p. 397.
21. K.-T. PARK, E. J. LAVERNIA and F. A. MOHAMED, *Acta Metall. Mater.* **42** (1994) 667.
22. Y. LI, S. R. NUTT and F. A. MOHAMED, *Acta Mater.* **45** (1997) 2607.
23. Y. LI and T. G. LANGDON, *Metall. Mater. Trans.* **29A** (1998) 2523.
24. L. KLOC, S. SPIGARELLI, E. CERRI, E. EVANGELISTA and T. G. LANGDON, *Acta Mater.* **45** (1997) 529.
25. L. KLOC, E. CERRI, S. SPIGARELLI, E. EVANGELISTA and T. G. LANGDON, *Mater. Sci. Eng.* A **216** (1996) 161.
26. K.-T. PARK, E. J. LAVERNIA and F. A MOHAMED, *Acta Metall. Mater.* **38** (1990) 2149.
27. K.-T. PARK and F. A. MOHAMED, *Metall. Mater. Trans.* **26A** (1995) 3119.
28. Y. LI and F. A. MOHAMED, *Acta Mater.* **45** (1997) 4797.
29. Y. LI and T. G. LANGDON, *Mater. Sci. Eng.* A **245** (1998) 1.
30. *Idem.*, *Acta Mater.* **46** (1998) 1143.
31. J. W. MARTIN, in "Micromechanisms in Particle-Hardened Alloys" (Cambridge University Press, Cambridge, 1980) p. 62.

Received 5 December 2001
and accepted 17 May 2002